

# Modeling of Wideband Mobile Radio Channels Based on Propagation Measurements

Werner Mohr

SIEMENS AG, OEN MN P 36  
Hofmannstrasse 51, D-81359 Munich, Germany

**ABSTRACT** - Synthetic models of the wideband mobile radio channel are required for mobile radio system design and optimization based on simulations. Additionally wideband models are implemented into hardware channel simulators which approximate the physical radio channel for experimental investigations. These models mainly correspond to a transversal filter structure. They are described by a small set of parameters like tap delays, statistics of the tap amplitudes and their corresponding Doppler spectra. Additionally long-term fading and distance dependence can be implemented. For the derivation of such models from a set of wideband measured complex impulse responses a mathematical heuristical approach is presented to determine these model parameters for a given number of taps with constant delays. Every tap is described by its complex time-varying amplitude including its statistic and Doppler spectrum. Additionally long-term fading due to shadowing and distance dependence are taken into account. The procedure yields a reasonable model for a given wideband measured radio channel to approximate the statistical properties of the physical channel.

## 1. Introduction

Wideband synthetic models of the mobile radio channel are required for mobile radio system design and optimization based on simulations to save computation time compared to the stored channel approach [1; 2]. Additionally wideband models are implemented into hardware channel simulators [e.g. 3] for experimental investigations. These models which are based on a transversal filter structure with a limited number of taps should only use a small set of parameters like the model tap delays, the tap amplitude statistics and the corresponding Doppler spectra [e.g. 4]. Measurements support this approach, because the number of significant paths with time-varying amplitude is constant in practical cases with nearly constant delays along a measurement route of a few 100 m in homogeneous scenarios.

Special methods like Prony [e.g. 5] approximate single measured impulse responses for a given number of taps by optimizing the delays and tap amplitudes in the least mean squares sense. Due to the variations of the approximated tap delays in consecutive channel impulse responses using such methods the Doppler spectra of the different taps within a set of impulse responses can not be calculated. Therefore a mathematical heuristical approach has been developed within the RACE-II Project ATDMA to be applied to pico-, micro- and macrocell scenarios. This method yields for a given number of model taps constant delays for a set of consecutive impulse responses. Every tap is described by its complex amplitude including the statistical distributions and Doppler spectra. The model parameters are obtained from a given set of measured consecutive channel impulse responses which are spaced equidistantly in time. This set ensures the spatial sampling theorem with respect to the Doppler shifts. Due to the limited measurement bandwidth the radio channel is approximated within this bandwidth. Additionally long-term fading effects due

to shadowing and distance dependence are taken into account. It is not required that the model approximates single measured impulse responses as accurate as possible. However the model represents the statistical properties and the Doppler spectra of the physical channel with sufficient accuracy.

## 2. Results of Wideband Propagation Measurements

Propagation measurements using a wideband channel sounder yield a set of  $K$  consecutive complex impulse responses  $h(\tau, t)$  starting with  $K = 0$  at  $t = t_1$  (Fig. 1). They are spaced equidistantly in the observation time domain by  $\Delta t$ . The measurement duration in the delay domain ( $\tau$ ) of every impulse response corresponds to  $\tau_N$ . To ensure the evaluation of Doppler spectra it is required to measure in minimum two impulse responses per RF carrier wavelength for constant mobile speed [6] to fulfil the spatial sampling theorem. This set of  $K$  consecutive measured impulse responses represents the radio channel. The magnitudes of  $h(\tau, t)$  are scaled according to the local shadowing effects and the distance dependence.

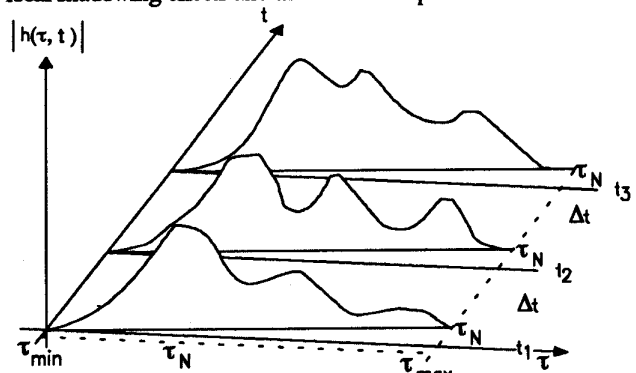


Fig. 1 Measured set of channel impulse responses

Every single impulse response is sampled according to the delay axis by  $N$  complex values. They are spaced by an equidistant time raster  $\Delta\tau$  which takes into account the sampling theorem in the equivalent low pass domain:

$$\Delta\tau = 1 / aB_{RF} \quad \tau_N = N\Delta\tau = N / aB_{RF} \quad (1)$$

$B_{RF}$  corresponds to the RF-measurement bandwidth and  $a$  to the oversampling factor. In the time discrete equivalent low pass representation a single measured impulse response at the observation instant  $t = k \Delta t + t_1$  with  $0 \leq k \leq K - 1$  is given by:

$$h(\tau, t) \rightarrow \sum_{n=0}^{N-1} \{h_r(n\Delta\tau, t) + jh_i(n\Delta\tau, t)\} \cdot \delta(\tau - n\Delta\tau) \quad (2)$$

This discrete representation of the radio channel with respect to the time and delay axis describes the channel in its bandwidth and Doppler behavior physically correct.

### 3. Methodology for the Derivation of Model Parameters

In the following the different steps of the method are described taking into account the principal statistical properties, the Doppler spectra, the long-term fading and distance dependence of the physical radio channel.

#### 3.1 Filtering of Channel Impulse Responses

A synthetic channel model with  $M$  distinct taps is based on the significant paths of the measured channel. The used channel sounder applies a rectangular window in the frequency domain for weighting the transfer function of the channel [7]. This window yields sidelobes in the impulse response which do not represent distinct paths of the radio channel. To obtain these paths every single impulse response is filtered in the frequency domain by a suitable window function  $W(n)$  [8]. A Hanning window is a good compromise between sidelobe reduction and broadening of the peaks which represent the paths.

$$W(n) = 0.5 + 0.5 \cdot \cos(2\pi n / N) \quad (3)$$

#### 3.2 Normalization of the Set of Impulse Responses

Due to shadowing effects and distance dependence a set of measured consecutive impulse responses does not represent in general a stationary scenario. The function  $l(r)d(r)$  corresponds to long-term fading  $l(r)$  due to shadowing and distance dependence  $d(r)$  versus the runlength  $r$  [9]. This step comprises a narrowband filtering of the wideband impulse responses and averaging with respect to a short sliding window  $w$  versus  $r$  to eliminate the short-term fading [10]. Due to the direct link between  $r$  and  $t$  the set of measured and filtered impulse responses  $h(\tau, t)$  is normalized by  $l(t)d(t)$  to obtain a more stationary situation [11] for statistical evaluations.

$$h_{nor}(\tau, t) = \sum_{n=0}^{N-1} \frac{\{h_r(n\Delta\tau, t) + jh_i(n\Delta\tau, t)\}}{l(t) \cdot d(t)} \cdot \delta(\tau - n\Delta\tau) \quad (4)$$

The statistical properties of the long-term fading, the distance dependence and the short-term fading are not mixed due to this normalization procedure.

#### 3.3 Determination of the Model Tap Delay Values

According to the transversal filter structure the model consists of  $M < N$  desired distinct taps with delays  $\tau_m$ . Their calculation is based on the average power delay profile  $p(n\Delta\tau)$  [12, p. 184] of the set of  $K$  normalized impulse responses which follows from the original data including noise. Due to this averaging the noise influence is reduced. In the following in  $p(n\Delta\tau)$  only the significant part with suitable dynamic range is taken into account. The part below a threshold (Fig. 2) and the corresponding samples of all single impulse responses are set to zero.

$$\begin{aligned} |h(n\Delta\tau)|_{nor}^2 &= \frac{1}{K} \sum_{k=0}^{K-1} \frac{[h_r^2(n\Delta\tau, k\Delta t + t_1) + h_i^2(n\Delta\tau, k\Delta t + t_1)]}{[l(k\Delta t + t_1) \cdot d(k\Delta t + t_1)]^2} \\ &= p(n\Delta\tau) \quad \text{for } 0 \leq n \leq N-1 \end{aligned} \quad (5)$$

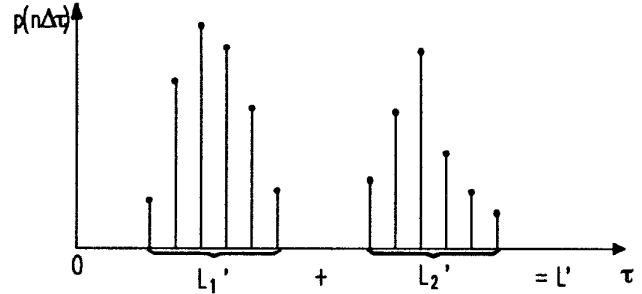


Fig. 2 Significant average power delay profile

Generally the remaining part of  $p(n\Delta\tau)$  with sample magnitudes  $> 0$  is shorter with  $L' < N$  samples than the originally measured noisy impulse responses. This part may exhibit distinct sections e.g. with  $L_1'$  and  $L_2'$  samples in the profile which must not be connected. The total length  $T_{L'}$  of these sections corresponds to

$$T_{L'} = L' \cdot \Delta\tau \quad (6)$$

To obtain the  $M$  delays  $\tau_m$  of the taps  $T_{L'}$  is subdivided into  $M$  intervals of equal length. If the result  $L'/M = I'$  is not an integer, samples with magnitude zero are added at suited locations to fulfil the equal length condition with an integer number  $I$  of samples. The algorithm for this subdivision depending on the distribution of remaining samples is described in [13]. The interval length should fulfil the condition using eq. (1)

$$I \cdot \Delta\tau > 2 / B_{RF} \quad \text{or} \quad I > 2a, \quad (7)$$

to obtain distinct taps according to  $B_{RF}$ . This procedure leads to the location of the  $M$  different intervals with respect to the index  $n$ . The first sample with the lowest index  $n$  starts with the index  $i_0$ ; the following intervals start at  $n = i_m$ . The model delay values  $\tau_m$  follow from the first moments of the average power delay profile in these intervals according to the delay  $\tau$ .

$$\tau_m = \sum_{n=i_m}^{i_m+I-1} n\Delta\tau \cdot p(n\Delta\tau) / \sum_{n=i_m}^{i_m+I-1} p(n\Delta\tau) \quad \text{for } 0 \leq m \leq M-1 \quad (8)$$

These  $\tau_m$  are generally not equidistant in delay. They are calculated from the average power delay profile; however in the following they are applied to every single impulse response.

#### 3.4 Approximation of the Single Impulse Responses

According to eq. (4) every single normalized impulse response is described by  $N$  or  $L'$  complex samples respectively. Every of the  $M$  intervals is characterized by  $I$  samples spaced by  $\Delta\tau$ . In the model these impulse responses are represented by  $M$  taps with delays  $\tau_m$  and complex amplitudes. The complex tap amplitude for interval  $m$  yields in the frequency domain the average phase and the same power contribution like the spectrum of the  $I$  samples within interval  $m$ . A suitable approximation of this phase by the complex tap amplitude is obtained by minimizing the error between both spectra in the least mean square sense within  $B_{RF}$ . The same power contribution is ensured by an additional scaling factor. The vectorially gathered complex amplitude  $h'/l(t)d(t)$

within interval  $m$  follows for impulse response  $k$  at delay  $\tau_m$  and fixed observation instant  $k\Delta t + t_1$  according to eq. (9).

$$\frac{h_r'(\tau_m, k\Delta t + t_1) + jh_i'(\tau_m, k\Delta t + t_1)}{l(k\Delta t + t_1) \cdot d(k\Delta t + t_1)} = \sqrt{\frac{\sum_{n=i_m}^{i_m+1-1} \{h_r^2(n\Delta\tau) + h_i^2(n\Delta\tau)\}}{h_r'^2(\tau_m) + h_i'^2(\tau_m)}} \cdot \frac{\{h_r^*(\tau_m) + jh_i^*(\tau_m)\}}{l(k\Delta t + t_1) \cdot d(k\Delta t + t_1)} \quad (9)$$

$$h_r^*(\tau_m) + jh_i^*(\tau_m) = \sum_{n=i_m}^{i_m+1-1} \{h_r(n\Delta\tau) + jh_i(n\Delta\tau)\} \cdot \frac{\sin\left[\frac{\pi}{a\Delta\tau}(n\Delta\tau - \tau_m)\right]}{\pi \frac{n\Delta\tau - \tau_m}{a\Delta\tau}}$$

This calculation has to be performed independently for every of the  $M$  intervals within one single impulse response and for all single impulse responses within the set of  $K$  impulse responses. From this procedure reasonable values for the  $M$  complex tap amplitudes are obtained. In the resulting model it is assumed, that the  $M$  distinct taps are caused by Gaussian wide-sense stationary uncorrelated scatterers (GWSSUS channel model) [14].

### 3.5 Statistics of the Complex Tap Amplitudes

For every of the  $M$  taps the amplitude distribution versus observation time  $t$  is investigated to take into account the statistical properties of the normalized radio channel with respect to the conditions for a stationary scenario (sec. 3.2).

For line-of-sight situations at delay  $\tau_0$  ( $m = 0$ ) or one dominant partial path at delay  $\tau_m$  ( $m \geq 1$ ) a Rice distribution is expected for the magnitude of the tap amplitude  $|h_{nor}(\tau_m)| = h_m$ ; for non line-of-sight situations at delay  $\tau_m$  with  $m \geq 0$  a Rayleigh-distribution is expected for the tap amplitude [15, pp. 156].

$$pdf(|h_m|) = \frac{|h_m|}{\sigma_m^2} e^{-\frac{|h_m|^2 + H^2}{2\sigma_m^2}} I_0\left(\frac{H|h_m|}{\sigma_m^2}\right) \quad \text{for } h_m \geq 0 \quad (10)$$

$$pdf(|h_m|) = \frac{|h_m|}{\sigma_m^2} e^{-\frac{|h_m|^2}{2\sigma_m^2}} \quad \text{for } h_m \geq 0 \quad (11)$$

$H$  corresponds to the tap magnitude without fluctuations and  $\sigma_m^2$  to the mean power of the fluctuation process. Rayleigh distributed samples are generated, if the quadrature components of the samples are Gaussian distributed values with variance  $\sigma_m^2$ . Rician distributed values are obtained, if an additional direct component is superposed vectorially to two orthogonal Gaussian distributed values with variance  $\sigma_m^2$  of the fluctuating components [15, pp. 160]. The ratio  $k = H/\sigma_m$  characterizes the Rician distribution. The advantage of these distribution functions is their simple generation compared to the more general description by the Nakagami- $m$  distribution which has more degree of freedom [12, p. 153].

The statistical evaluation for the probability density distribution functions (pdf) and the cumulative distribution functions (cdf) as well is performed for all delays  $\tau_m$  from the magnitude of the

gathered samples according to eq. (9) versus the whole set of  $K$  normalized impulse responses.

$$pdf\{\dots\} \quad \text{or} \quad cdf\left\{\sqrt{h_r'^2(\tau_m) + h_i'^2(\tau_m)} / l \cdot d\right\} \quad (12)$$

These obtained distribution functions for the  $M$  model taps are fitted to the distribution functions (eqs. (10) or (11)) using the first and second moment of the measured amplitude distribution compared to the corresponding values for the Rice distribution [15, p. 160].

$$\frac{E^2\{|h_m|\}}{E\{|h_m|^2\}} = \frac{\frac{\pi}{2} \cdot e^{-k^2/2} \cdot \left[ \left(1 + \frac{k^2}{2}\right) \cdot I_0\left(\frac{k^2}{4}\right) + \frac{k^2}{2} \cdot I_1\left(\frac{k^2}{4}\right) \right]^2}{2 + k^2}$$

$$\sigma_m^2 = E\{|h_m|^2\} / (2 + k^2) \quad (13)$$

$$H = k \cdot \sigma_m$$

These statistical values of the tap amplitudes are varying versus  $t$  according to the Doppler spectra of the  $M$  taps. In the model it is only required to obtain one representative with the derived statistical properties out of the variety of possible processes.

### 3.6 Doppler Spectra of the $M$ Different Taps

The variations of  $h_r'$  and  $h_i'$  versus  $t$  for fixed delay  $\tau_m$  are determined by movements in the surroundings but mainly of the mobile itself. This is represented by the Doppler spectra of the  $M$  taps in the sense of short term Doppler spectra. For determining the spectrum of tap  $m$  the total runlength is subdivided into  $P$  non overlapping bursts of about 5 - 10 m in microcells and 10 - 20 m in macrocells. The short term Doppler spectrum of burst  $p$  is given by Fourier transformation of the set of  $O = K/P$  impulse responses per burst:

$$S_{D,p}\left(\tau_m, 2\pi \frac{l}{O\Delta t}\right) = \Delta t \sum_{k=(p-1)O}^{pO-1} \frac{\{h_r'(\tau_m, k\Delta t + t_1) + jh_i'(\tau_m, k\Delta t + t_1)\}}{l(k\Delta t + t_1) \cdot d(k\Delta t + t_1)} \cdot e^{-j2\pi \frac{kl}{O}}$$

$$\text{for } 1 \leq p \leq P \quad (14)$$

An estimate of its power density spectrum is obtained by averaging the magnitude squares of these Doppler spectra:

$$\left|S_D\left(\tau_m, 2\pi \frac{l}{O\Delta t}\right)\right|^2 = c \cdot \sum_{p=1}^P \left|S_{D,p}\left(\tau_m, 2\pi \frac{l}{O\Delta t}\right)\right|^2 \quad (15)$$

For implementing these Doppler spectra into the model only their shape is required to generate a channel representation with similar statistical and Doppler behavior like the measured channel. Generally these spectra are asymmetrical with respect to zero Doppler shift  $\omega_D$  due to irregularly distributed angles of incidence and different amplitudes of the partial received waves. Therefore the time function of the real part  $h_r'/ld$  is correlated to the imaginary part  $h_i'/ld$ . In the synthetic model these Doppler spectra of the fluctuating components are generated using a suitable filter structure and two uncorrelated Gaussian noise

processes with zero mean and two-sided noise power density  $N_0 = 1$  of  $n_c$  and  $n_s$  [15, pp. 112].

$$n_c(t) + jn_s(t) \quad (16)$$

Based on their autocorrelation and crosscorrelation functions

$$\begin{aligned} R_{cc}(\Delta t') &= R_{ss}(\Delta t') = N_0 \cdot \delta(\Delta t') \\ R_{cs}(\Delta t') &= R_{sc}(\Delta t') = 0 \end{aligned} \quad (17)$$

and the filter structure  $G(\omega_D)$  in Fig. 3 the magnitude square of the Doppler spectra is given by

$$|S_D(\omega_D)|^2 = 2 \cdot N_0 \cdot |G(\omega_D)|^2 \quad (18)$$

The scaling factor  $c$  in eq. (15) ensures the mean power  $\sigma_m^2$  of the fluctuating component of tap  $m$  according to sec. 3.5.

$$\sigma_m^2 = \frac{c}{2\pi} \int_{-\infty}^{\infty} \sum_{p=1}^P |S_{D,p}(\tau_m, \omega_D)|^2 d\omega_D = \frac{N_0}{\pi} \int_{-\infty}^{\infty} |G(\tau_m, \omega_D)|^2 d\omega_D \quad (19)$$

Due to eq. (18) the phase of  $G(\omega_D)$  can be chosen arbitrarily with  $\varphi(\omega_D) = 0$ . The system functions in Fig. 3 follow directly from the even and odd component of  $|S_D(\omega_D)|^2$ :

$$\begin{aligned} G(j\omega_D) &= |G(\omega_D)| e^{j\varphi(\omega_D)} = \sqrt{|S_D(\omega_D)|^2 / 2N_0} \\ G_{\text{even}}(j\omega_D) &= [G(j\omega_D) + G(-j\omega_D)] / 2 \quad \bullet - \circ \quad g_r(t) \quad (20) \\ G_{\text{odd}}(j\omega_D) &= [G(j\omega_D) - G(-j\omega_D)] / 2 \quad \bullet - \circ \quad jg_i(t) \end{aligned}$$

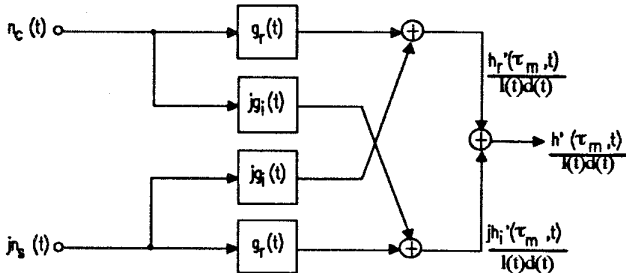


Fig. 3 Filter structure for generating given Doppler spectra

A dominant component in the Rice case is added to the Doppler spectrum by a discrete line with amplitude  $H$  and arbitrary or user defined Doppler shift  $\omega_{Dm}$ .

#### 4. Radio Channel Model

Fig. 4 shows the principal channel model using  $M$  taps with complex time varying amplitudes. The transversal filter within the model is normalized with respect to  $l(t)$  and  $d(t)$  of the measured set of impulse responses. In this example it is assumed that the amplitude of the first tap exhibits a Rician distribution. The other taps are Rayleigh distributed. The time varying tap amplitudes are generated using complex Gaussian noise processes. Their statistical parameters are obtained according to sec. 3.5. These processes are filtered by Doppler filters - the discrete line of a dominant component is added at the output of the Doppler filter - to obtain representatives of the required

Doppler spectra. At the input of the model time functions for the correlated log-normal distributed long-term fading  $l(t)$  and the distance dependence  $d(t)$  are introduced by a multiplicative frequency independent component.

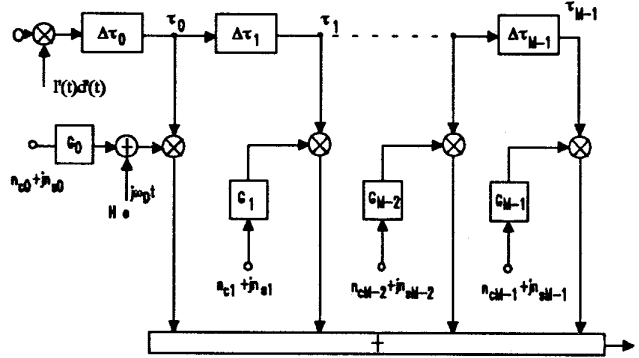


Fig. 4 Structure of the synthetic radio channel model

The entire model represents a channel according to the eqs. (2) and (4) with in general not equidistant time shifted taps with time varying amplitudes including the influence of long-term fading and distance dependence.

#### 5. Example for Channel Modeling

This example corresponds to a macrocell scenario which is located in hilly terrain with a base station on the top of a hill. The mobile station has moved in a forest away from the base station. After applying the normalization according to eq. (4) the set of measured impulse responses is shown in Fig. 5.

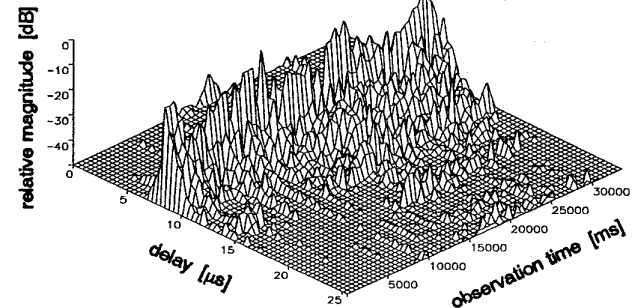


Fig. 5 Normalized set of measured impulse responses

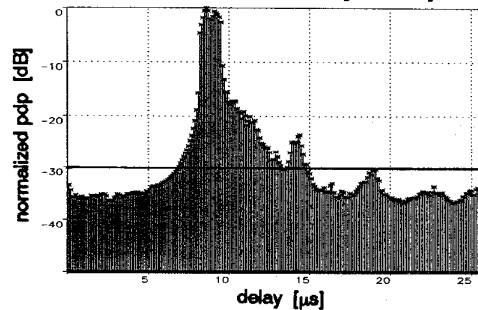


Fig. 6 Average power delay profile (pdp) of the measured set

In this example the samples of the average power delay profile (eq. (5)) are taken into account within a dynamic range of 30 dB (Fig. 6). For  $M = 6$  taps Fig. 7 shows the average power delay

profile of the model. The obtained model parameters are summarized in Table 1. In this case the Doppler spectra of all  $M$  taps are asymmetrical with the main power contribution for negative Doppler shift depending on this special scenario. Fig. 8 shows the exemplary spectrum for the main tap 2.

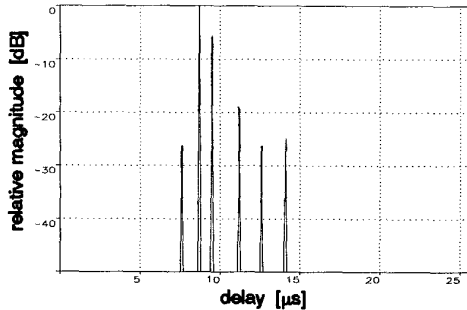


Fig. 7 Average power delay profile of the model

tap No.	$\tau_m$ [ $\mu$ s]	pdf	k	$\sigma_m$	H	rel. tap ampl. [dB]
1	0.000	Rayleigh	0.0	473353.6	0.0	-25.9
2	1.278	Rayleigh	0.0	9360228.0	0.0	0.0
3	2.053	Rayleigh	0.0	5035276.5	0.0	-5.4
4	3.913	Rayleigh	0.0	1078813.6	0.0	-18.8
5	5.466	Rice	1.2	357068.9	430000.7	-26.0
6	6.773	Rayleigh	0.0	585265.2	0.0	-24.1

Table 1 Model parameters

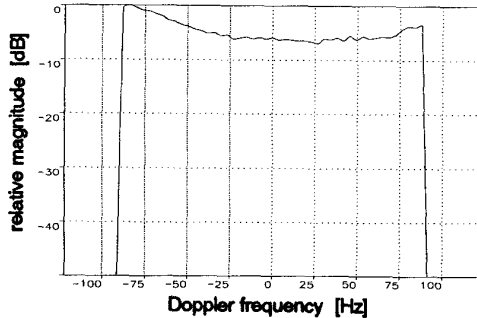


Fig. 8 Doppler spectrum of the main tap No. 2

## 6. Conclusion

This modeling procedure follows a mathematical heuristical approach and is based on wideband propagation measurements. The model comprises a transversal filter structure of degree  $M$  with non equidistant time shifted taps including long-term fading and a distance dependence. Their complex amplitudes are time varying according to the corresponding Doppler spectra and statistical distributions. The accuracy depends on the degree  $M$  with respect to the measured radio channel. In the example the applicability of this approach is presented.

## Acknowledgement

This work has been partially funded by the Commission of the European Communities in the RACE program (Research and development in Advanced Communications technologies in Europe) under the RACE 2084 ATDMA Project. The author would like to acknowledge the

contributions of his colleagues from ALCATEL Mobile Communication France, ALCATEL Standard Eléctrica S.A., DeTeMobil, Fondazione Ugo Bordoni, Nokia Mobile Phone and Nokia Research Center, Roke Manor Research, SIEMENS AG, Télécom Paris, Universidad Politécnica de Cataluña, The University of Strathclyde and especially the colleagues of Deutsche Telekom AG, ESG Elektronik-System-Gesellschaft mbH and France Télécom CNET for the very worthy discussions, although the views expressed are those of the author and do not necessarily represent those of the project as a whole.

The author would like to thank Mrs. C. Büchel Marques dos Reis from Instituto Superior Técnico, Lisbon, Portugal for improving the method and implementing the software.

## References

- [1] Hagenauer, J. and W. Papke: Der gespeicherte Kanal - Erfahrungen mit einem Simulationsverfahren für Fading-Kanäle. *Frequenz*, vol. 36, 1982, No. 4/5, pp. 122 - 129.
- [2] Lorenz, R.W.: Zeit- und Frequenzabhängigkeit der Übertragungsfunktion eines Funkkanals bei Mehrwegeausbreitung mit besonderer Berücksichtigung des Mobilfunkkanals. *Der Fernmelde-Ingenieur*, vol. 39, 1985, No. 4.
- [3] Lecours, M. and Fr. Marceau: Design and Implementation for a Channel Simulator for Wideband Mobile Radio Transmission. 39th IEEE Vehicular Technology Conference, San Francisco, Ca, USA, 1 - 3 May 1989, pp. 652 - 655.
- [4] ITU - Radiocommunication Study Group: Final Report on RF Channel Characterization. The Joint Technical Committee of Committee T1 T1P1.4 and the T1A TR46.3.3/TR45.4.4 on Wireless Access, JTC(AIR)/93.09.23 - 238R2, 18.10.1993.
- [5] Hewitt, A., W.H. Lau, J. Austin and E. Vilar: An Autoregressive Approach to the Identification of Multipath Ray Parameters from Field Measurements. *IEEE Trans. on Communications*, vol. 37, No. 11, 1989, pp. 1136 - 1143.
- [6] Kadel, G. and R.W. Lorenz: Breitbandige Ausbreitungsmessungen zur Charakterisierung des Funkkanals beim GSM System. *Frequenz*, vol. 45, Nr. 7 - 8, pp. 158 - 163.
- [7] Felhauer, T., P.W. Baier, W. König and W. Mohr: Optimized Wideband System for Unbiased Mobile Radio Channel Sounding with Periodic Spread Spectrum Signals. *IEICE Trans. Communications*, vol. E76-B, No. 8, 1993, pp. 1016 - 1029.
- [8] Harris, J.: On the use of windows for harmonic analysis with the discrete Fourier Transform. *Proc. of the IEEE*, vol. 66, No. 1, 1978, pp. 51 - 83.
- [9] Gollreiter, R. et. al: Channel Models Issue 2. RACE-II ATDMA, R2084/ESG/CC3/DS/P/029/b1, May 1994.
- [10] Lee, W.C.Y.: Estimate of Local Average Power of a Mobile Radio Signal. *IEEE Transactions on Vehicular Technology*, vol. 34, No. 1, 1985, pp. 22 - 27.
- [11] Clarke, R.H.: A Statistical Theory of Mobile-Radio Reception. *BSTJ*, vol. 47, 1969, pp. 957 - 1000.
- [12] Parsons, J.D.: *The Mobile Radio Propagation Channel*. Pentech Press Publishers, London, 1992.
- [13] Büchel Marques dos Reis, C.: *Modelling of Mobile Radio Channels Based on Wideband Propagation Measurements*. Master Thesis, Instituto Superior Técnico, Lisbon, Portugal and Siemens AG, Munich, Germany, 1994.
- [14] Bello, P.A.: Characterization of Randomly Time-Variant Linear Channels. *IEEE Trans. on Communications*, vol. COM-11, 1963, No. 12, pp. 360 - 393.
- [15] Thomas, J.B.: *An Introduction to Statistical Communication Theory*. John Wiley & Sons, New York, 1969.